JOURNAL OF
APPLIED
CRYSTALLOGRAPHY

ISSN 1600-5767

Sub-millisecond time-resolved small-angle neutron scattering measurements at NIST

Charles Glinka,[a,b]* Markus Bleuel,[a] Peter Tsai,[a] Dominika Zákutná,[c]‡ Dirk Honecker,[d] Dominique Dresen,[c] Flore Mees[c] and Sabrina Disch[c]

[a]Center for Neutron Research, National Institute of Standards and Technology, 100 Bureau Drive/MS 6103, Gaithersburg, Maryland 20899, USA, [b]Chemical and Biomolecular Engineering, University of Delaware, 150 Academy Street, Newark, DE 19716, USA, [c]Department für Chemie, Universität zu Köln, 116 Luxemburger Strasse, 50939, Köln, 50939, Germany, and [d]Physics and Materials Science Research Group, University of Luxembourg, 162a Avenue de la Faïencerie, Grand Duchy of Luxembourg, L-1511, Luxembourg. *Correspondence e-mail: charles.glinka@nist.gov

Received 6 December 2019
Accepted 30 March 2020

Edited by G. J. McIntyre, Australian Nuclear Science and Technology Organisation, Lucas Heights, Australia

‡ Present address: Department of Inorganic Chemistry, Charles University in Prague, Hlavova 2030/8, Prague 2, Czech Republic.

Keywords: small-angle neutron scattering; hematite nanospindles; time-involved small-angle neutron experiments; TISANE; reorientation dynamics; magnetic particles.

Supporting information: this article has supporting information at journals.iucr.org/j

Instrumentation for time-resolved small-angle neutron scattering measurements with sub-millisecond time resolution, based on Gähler's TISANE (time-involved small-angle neutron experiments) concept, is in operation at NIST's Center for Neutron Research. This implementation of the technique includes novel electronics for synchronizing the neutron pulses from high-speed counter-rotating choppers with a periodic stimulus applied to a sample. Instrumentation details are described along with measurements demonstrating the utility of the technique for elucidating the reorientation dynamics of anisometric magnetic particles.

1. Introduction

In the late 1990s R. Gähler (Kipping *et al.*, 2008) proposed a new technique that he termed TISANE, for time-involved small-angle neutron experiments, for achieving sub-millisecond time resolution in small-angle neutron scattering (SANS) measurements. The technique is applicable to systems that respond to a periodic stimulus (*e.g.* oscillatory stress, magnetic or electric fields) but does require accumulation of data over many oscillation cycles to obtain adequate counting statistics. The technique utilizes high-speed choppers upstream from the instrument's collimation to emit neutron pulses with microsecond burst times. The frequency of these bursts, in relation to the sample stimulus frequency, results in time focusing at the detector which gives the technique a considerable efficiency advantage over traditional time-of-flight measurements.

The TISANE technique has been implemented at only a few neutron centers worldwide (Wiedenmann *et al.*, 2006; Mühlbauer *et al.*, 2009). Here we describe its installation and operation at NIST's Center for Neutron Research (NCNR). The technique requires either a highly stable reference frequency for controlling the choppers, sample stimulus and detector time base, or, as is the case at NIST, novel electronics that correct for small drifts in either the neutron pulse or sample stimulus frequencies from their nominal values. Measurements demonstrating the time resolution attainable with the NIST apparatus are presented. Preliminary measurements are also presented that demonstrate the utility of the technique for probing the reorientation dynamics of anisometric nanoparticles in an oscillating magnetic field.

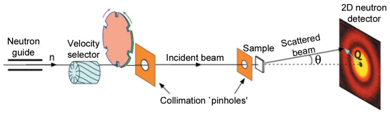

https://doi.org/10.1107/S1600576720004367

2. TISANE implementation at NIST

The principle of TISANE is illustrated in Fig. 1 and described in detail in the work of Kipping *et al.* (2008).

The key component needed for TISANE is a pair of high-speed counter-rotating disc choppers to pulse the neutron beam upstream from the pinhole collimation as depicted in Fig. 2. These have been installed on the 30 m SANS instrument (Glinka *et al.*, 1998) on neutron guide NG-7 at the NCNR. Further details about the choppers are given in Appendix *A*.[1]

The relationship between the neutron pulse frequency, f_c, the sample stimulus frequency, f_s, and the detector reset ($t = 0$) frequency, f_d, which follows from the TISANE conditions given in the equations in Fig. 1 is

$$f_d = f_s - f_c. \tag{1}$$

Maintaining the condition in equation (1) over a period of hours, as is often necessary to accumulate enough neutron counts to have well defined SANS patterns for each of ten to 20 time bins, requires either extreme stability of all three frequencies, or the capability to continuously monitor f_s and f_c and recalculate f_d as needed to satisfy equation (1). The latter approach is used at the NCNR and is implemented through a custom piece of electronics, referred to as the detector trigger generator (DTG), described in detail in Appendix *B*. Taking this approach provides greater flexibility in being able to adapt the technique to a user's sample-environment equipment. A user need only provide a sample frequency stable to ~0.1% and the DTG ensures that equation (1) will be satisfied over the course of a measurement.

2.1. Performance measurements

Three factors affect the time resolution in a TISANE measurement: (i) the neutron burst width (in time) which depends on the chopper speeds; (ii) the thickness of the sample, which blurs the time a neutron scatters from the sample; and (iii) the thickness of the detector detection volume, which blurs the time a neutron is detected. These three factors are independent and hence add in quadrature to give the overall time resolution at the detector as (Wiedenmann *et al.*, 2006)

$$\Delta T_D^2 = \left(\Delta T_c \frac{L_2}{L_1}\right)^2 + \left(\Delta T_s \frac{L_1 + L_2}{L_1}\right)^2 + \Delta T_d^2 \tag{2}$$

where ΔT_c is the FWHM of the neutron burst, ΔT_s is the uncertainty in the interaction time at the sample and ΔT_d is the uncertainty in the detection time at the detector. The last two terms depend on the sample, l_s, and detector thickness, l_d, respectively, and the mean neutron speed, v_n,

$$\Delta T_s \cong l_s/v_n, \quad \Delta T_d \cong l_d/v_n. \tag{3}$$

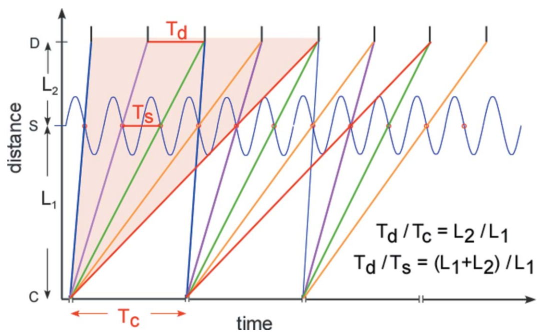

Figure 1
A time–distance diagram showing the trajectories of neutrons from successive chopper openings (C) resulting in frame overlap at the sample (S) and detector (D). L_1 is the chopper-to-sample distance and L_2 is the sample-to-detector distance. The sine wave represents the periodic stimulus applied to the sample. The shaded region represents the range in trajectories in one pulse, which has a broad distribution of wavelengths determined by the upstream velocity selector (typical $\Delta\lambda/\lambda$ = 22%). Neutrons from different chopper pulses which probe the same oscillation state when they reach the sample are collected in equivalent time channels at the detector (D), if the equations in the diagram are satisfied.

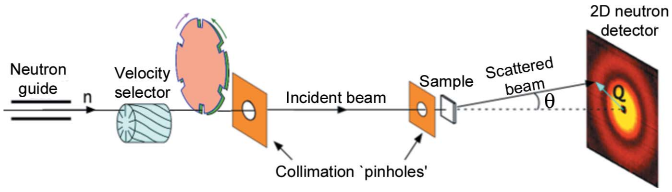

Figure 2
Schematic diagram of the SANS instrument showing the location of the two counter-rotating disc choppers used to perform TISANE measurements.

In most cases the terms in equation (3), which lie in the range 1–5 µs, are much smaller than the neutron burst time. Hence the overall resolution is dominated by the first term in equation (2).

To measure the time resolution of the TISANE apparatus a 'mini-chopper' was set up at the sample position. This small disc chopper had eight, 1 mm-wide, slots to simulate a sharply peaked periodic sample response function. A fixed 1 mm-wide slit, 15 mm high, defined the beam size incident on the mini-chopper. Neutrons passing through these slots, despite their different wavelengths, should arrive at equivalent times at the detector if the TISANE conditions [Fig. 1 and equation (1)] are satisfied.

Fig. 3(*a*) shows data collected with the counter-rotating choppers spinning at 53 Hz, giving a neutron burst frequency f_c = 320 Hz (six pulses per revolution). For this measurement the distance between these choppers and the mini-chopper was L_1 = 15.2 m and the distance from the mini-chopper to the detector was L_2 = 13.5 m. The corresponding sample slot frequency, $f_s = f_c(L_1 + L_2)/L_2$, was f_s = 680 Hz. For this measurement the chopper burst time, FWHM, was

$$\Delta T_c = \frac{6w}{2\pi(2f_c)r} = 310 \ \mu\text{s}, \tag{4}$$

---

[1] Disclaimer. Certain commercial equipment, instruments, or materials are identified in this paper to adequately describe methods and technology used in this work. Such identification does not imply recommendation or endorsement by the National Institute of Standards and Technology, nor does it imply that the materials or equipment identified are necessarily the best available for the purpose.

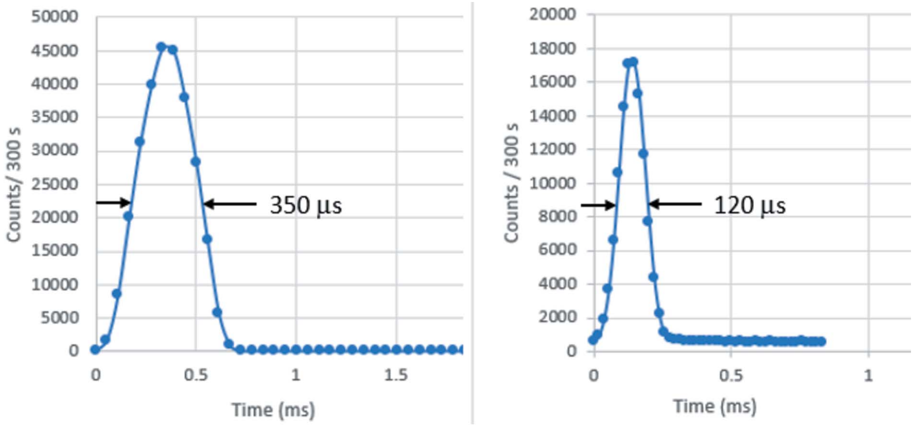

(*a*) (*b*)

Figure 3
TISANE measurements of the neutron bursts from a rotating 'mini-disc chopper' at the sample position of the SANS instrument. In both cases the width of the peaks is mostly due to the burst time of the pulses from the TISANE choppers upstream. In (*a*) the pulse frequency at the sample was f_s = 680 Hz. The choppers rotated with the same frequency (3200 r min^{-1}) giving a burst time [see equation (9)] of 310 µs, a burst period of 2.8 ms and a calculated FWHM at the detector from equation (2) of 285 µs, about 20% less than the observed width of 350 µs. In (*b*) the pulse frequency at the sample was f_s = 1020 Hz. The chopper frequencies were in a 3/2 ratio (14 400 and 9610 r min^{-1}) giving a burst time of 82 µs, a burst period of 2.1 ms and a calculated FWHM at the detector of 87 µs, about 30% less than the observed width of 120 µs. These data demonstrate the improvement in the ratio of peak width to peak period achievable by running the choppers at different speeds with the appropriate speed ratio (see Appendix *B* for further details).

where w = 50 mm is the width of the slots in the counter-rotating choppers; r = 240 mm is the radial distance of the slots from the axis of rotation (see Appendix *A*). Similarly,

$$\Delta T_s = \frac{8w_s}{2\pi(f_s)r_s} = 38\ \mu\text{s}, \qquad (5)$$

where w_s = 1 mm is the slot width in the mini-chopper, r_s = 50 mm is its radius and $f_s/8$ is its rotation frequency (eight slots in the disc). Hence the overall calculated FWHM of the peak observed at the detector is, from equation (2), ΔT_D = 285 µs. As seen in Fig. 3(*a*), the observed FWHM is about 20% larger than calculated.

Fig. 3(*b*) shows another data set taken with the counter-rotating discs running at different speeds with a speed ratio of 3/2. As described in Appendix *A*, running the choppers at rational-fraction ratios is a way of further improving the time resolution but with a corresponding reduction in the duty cycle. For this measurement f_s = 1020 Hz and f_c = 480 Hz. The peak width calculated from equation (2) is then 87 µs, about 30% less than the observed width.

3. Probing reorientation dynamics of anisometric nanoparticles

TISANE measurements at the ILL have been used to probe the response of a colloidal dispersion of Ni nanorods to an oscillating magnetic field (Bender *et al.*, 2015). Here we report TISANE measurements in an applied magnetic field carried out at the NCNR on a system of anisometric nanoparticles with significantly different reorientation behavior. The sample in this case consisted of hematite nanospindles with a mean length of 326 (1) nm and mean particle diameter of 54 (1) nm, dispersed in D_2O. Hematite spindles are known to orient with their long axis perpendicular to an applied field as the magnetic easy axis lies in the basal plane of the hematite crystal structure (Reufer *et al.*, 2010). In a previous study the magnetic moment was found to fluctuate thermally around the magnetic easy axis within the basal plane, whereas the morphological orientation distribution of the spindles in an applied magnetic field is still very well described by the Boltzmann distribution (Zákutná *et al.*, 2019). Thus, with a horizontal static magnetic field of H_{DC} = 37 mT perpendicular to the neutron beam, the spindles are expected to preferentially align normal to the magnetic field, *i.e.* in the plane spanned by the vertical direction and the neutron beam direction. By superposing a sinusoidal magnetic field in the vertical direction with an amplitude of H_{AC} = 8 mT, the effective magnetic field direction oscillated in the plane perpendicular to the neutron beam. The apparatus is shown in Fig. 4.

Time-resolved SANS measurements in the lower-frequency range were made with a continuous beam (also referred to as a stroboscopic mode; Wiedenmann *et al.*, 2006) with time-stamping relative to the period, T_s, of the oscillatory field. Such continuous SANS measurements were performed at field oscillation frequencies of 100, 200 and 300 Hz, whereas TISANE experiments were done at 425 and 690 Hz. Typical data collection times were 2 h for the continuous-beam measurements and 10 h for the TISANE measurements. Both continuous and TISANE measurements were binned into eight frames per period after acquisition. In Fig. 5 three frames taken at the different phases of the AC field are presented. From the 2D detector images the variation of the tilting angle

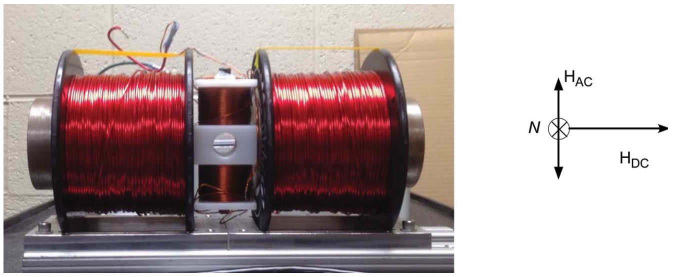

Figure 4
View in the neutron beam direction of the magnetic field setup with the sample located in the central opening. The larger pair of split coils, with iron inserts, provided a static horizontal magnetic field, H_{DC} = 37 mT. The smaller coils (no inserts) provided an oscillatory vertical field with an amplitude of H_{AC} = 8 mT.

is clearly visible with the anisotropic scattering pattern rotating clockwise and anticlockwise over the course of a period, which indicates that the spindle orientation follows the effective field vector at all times (for illustration, videos of all eight frames for each measured frequency are provided in the supporting information). Azimuthal scattering intensities at constant Q were extracted from the measured detector frames, integrating a Q range of 0.0025–0.0095 Å^{-1}. The spindle orientation with respect to the horizontal direction was parametrized via the maximal position of the azimuthal scattering intensities, which was determined using a $\cos^2\kappa$ function (where κ is the azimuthal angle between the horizontal direction and the scattering wavevector $\mathbf{Q}$). The obtained deflection angles over a period at different oscillating field frequencies are presented in Fig. 6(a).

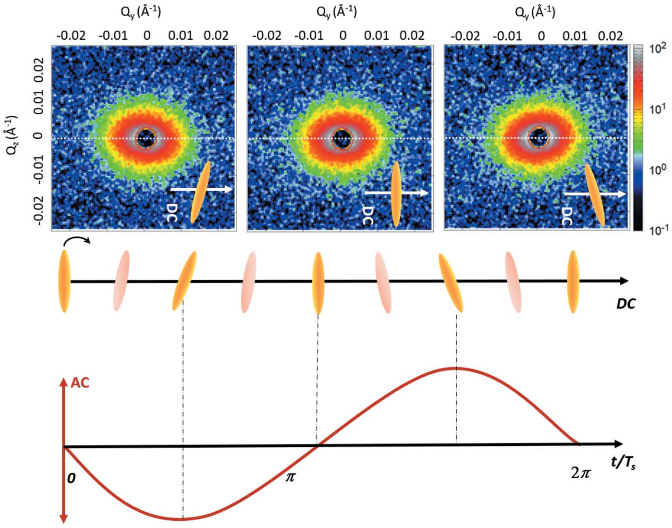

Figure 5
(Upper panel) 2D SANS detector images of different time frames at a frequency of 100 Hz. (Middle panel) Schematic representation of the spindles wobbling in the AC field direction. (Lower panel) AC field amplitude over the course of a period T_s. The maximal field strength is H_{AC} = 8 mT.

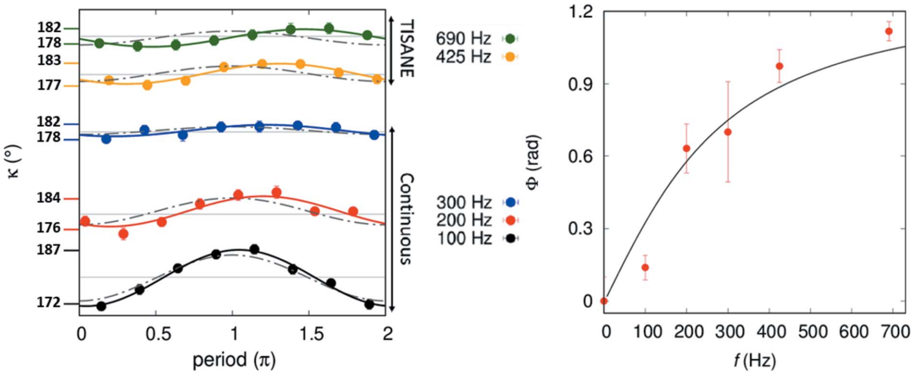

(a) (b)

Figure 6
(a) Variation of the oscillation amplitude over the period $T = 1/f$ at various frequencies. The phase of the inducing field (with arbitrary amplitude) is shown as a dot–dashed line. For 100, 200 and 300 Hz continuous beam measurements were performed and for 425 and 690 Hz measurements were done in TISANE mode. Numbers at the left axis correspond to the maximum and minimum deflection angle κ of the scattering. (b) Frequency dependence of the phase shift. The error bars represent the estimated standard deviations.

The oscillation amplitude decreases and nearly vanishes at 300 Hz, a behavior that originates from a combination of sample-related relaxation effects and the limited time resolution of the continuous SANS experiment with a wavelength spread of $\Delta\lambda/\lambda$ = 12%. TISANE measurements carried out at higher frequencies of 425 and 690 Hz reveal a time-dependent, oscillatory scattering signal again, with enhanced oscillation amplitude. This confirms the improved time resolution of the TISANE experiment, which allows tracking the phase shift up to higher frequencies. The obtained phase lag with respect to the AC field increases with AC frequency [Fig. 6(b)]. The larger error bar of the phase lag at 300 Hz is a result of the smearing of the amplitude caused by limited time resolution due to the wavelength spread of the continuous SANS experiment. The motion of the spindles can be described in terms of a periodically driven damped harmonic rotational oscillator with negligible inertia. The deflection κ is given by (Tschöpe *et al.*, 2014)

$$\kappa(t) = \frac{H_{AC} m_r}{\left[(-\xi_r\omega)^2 + (H_{DC} m_r)^2\right]^{1/2}} \times \cos\left[\omega t + \arctan\left(\frac{H_{DC} m_r}{-\xi_r\omega}\right)\right], \qquad (6)$$

with an oscillatory magnetic field $\mathbf{H} = (0, H_{DC}, H_{AC}\sin\omega t)$, the integral particle moment of spindles $m_r = 6.6 \times 10^{-19}$ J T^{-1}, rotational friction ξ_r and angular frequency ω of the oscillatory field. The rotational diffusion coefficient can be extracted from the obtained rotational friction according to the relation

$$D_r = k_B T/\xi_r, \qquad (7)$$

where T is temperature and k_B is the Boltzmann constant. From the fit of the frequency-dependent phase lag [Fig. 6(b)] according to the relation

$$\phi(f) = \arctan\left(\frac{H_{DC} m_r D_r}{-k_B T 2\pi f}\right), \qquad (8)$$

a rotational diffusion coefficient of D_r = 258 (50) s^{-1} was obtained. The determined rotational diffusion coefficient is in excellent agreement with theoretical estimates for an ellipsoid of revolution according to Perrin (Perrin, 1934; Wright & Baxter, 1976) (D_r = 239 s^{-1}), based on the morphological details of the nanospindles and the solvent viscosity.

4. Conclusions

Instrumentation for TISANE measurements is now fully operational at the NCNR. The counter-rotating disc choppers installed at the NG-7 30 m

SANS instrument have a maximum speed of 18 000 r min^{-1}, with six 50 mm-wide slots in each disc, corresponding to a maximum neutron pulse rate of 1800 Hz. At this pulse rate, the maximum accessible sample stimulus frequencies $f_s = f_c(1 + L_1/L_2)$ range from ~3600 Hz (L_2 = 15 m) to ~20 000 Hz (L_2 = 1 m). The corresponding lower frequencies, above which TISANE provides superior time resolution over continuous-beam time-resolved measurements, are ~50 Hz, for L_2 = 15 m, and ~300 Hz, for L_2 = 1 m (see Fig. 8). Performance measurements utilizing a disc chopper at the sample position with 1 mm-wide slits demonstrate the time focusing although the measured time resolution is 20–30% greater than that calculated from equation (2).

The implementation of TISANE at the NCNR is particularly well suited to user experiments owing to its relaxed requirement for the stability of the sample stimulus frequency. Custom electronics that continuously monitor the neutron pulse and sample stimulus frequency and send time-zero pulses to the detector to satisfy the TISANE condition in equation (1) enable measurements of several hours to be performed with no significant degradation in the quality of the data.

For hematite spindles with preferred orientation perpendicular to an oscillating magnetic field, the frequency-dependent phase lag of the orientation distribution was determined, which gives experimental insight into the rotational diffusion coefficient. The enhanced time resolution provided by TISANE allows tracking of the oscillatory motion of the polar particle axis up to high frequencies close to the kHz range, well beyond the limit set by the continuous SANS technique. Hence TISANE does not only qualify as a technique to assess orientational properties of anisometric nanoparticles in periodic perturbation. In addition, TISANE enables determination of the rotational diffusion of magneto- or electroactive complex nanosized fluids, where a conventional depolarized dynamic light scattering analysis is typically hampered by extended particle concentration and turbidity of the sample. Moreover, the TISANE technique complements X-ray photon correlation spectroscopy (Wagner *et al.*, 2013), measuring the translational diffusion on optically opaque suspensions.

APPENDIX *A*
TISANE mechanics

The NCNR's TISANE chopper system (Lindenau, 2003) has two identical counter-rotating discs in a single chopper vacuum enclosure (Fig. 7). The discs have six 50 mm-wide openings at a radius of 240 mm and are separated by 100 mm in the beam direction. The rotational speed and phasing between the discs can be adjusted independently. The choppers are 'open' when their slots coincide at the beam position. The discs have magnetic bearings and can be operated at speeds from ~3000 to 18 000 r min^{-1} (50–300 Hz).

As discussed in the text, the time resolution for TISANE is largely determined by the chopper open (or burst) time. The open time, $\Delta T_{\rm c}$ (FWHM), is determined by the chopper slot width, w (or the beam width, whichever is smaller), and the speeds of the chopper discs,

$$\Delta T_{\rm c} = \frac{w}{V_a + V_b} \qquad (9)$$

where V_a and V_b are the linear speeds of the two choppers at radius R = 240 mm. The speeds of the two choppers need not be the same, but must be related by $MV_a = NV_b$, where N and M are integers, in order for both discs to be open at the beam position at the same time. Hence,

$$\Delta T_{\rm c} = \frac{w}{V_a(1 + M/N)} \quad \text{and} \quad T_{\rm c} = \frac{Nd}{V_a} = \frac{Md}{V_b}$$

is the time between pulses where d = 251 mm as shown in Fig. 7. Hence the duty cycle is

$$\frac{\Delta T_{\rm c}}{T_{\rm c}} = \frac{w}{(M + N)d}. \qquad (10)$$

When $N = M = 1$, the choppers run at the same speed, there are six neutron pulses per revolution and the duty cycle is maximum at ~10%. $\Delta T_{\rm c}$ can be reduced, and the time

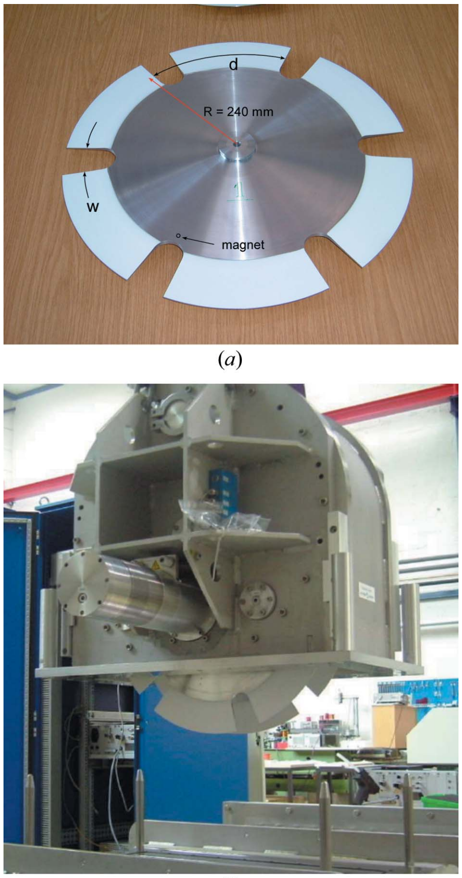

(*a*)

(*b*)

Figure 7
(*a*) One of two identical discs that counter-rotate inside the neutron chopper housing seen (*b*) being lowered into the SANS 15 m-long pre-sample vacuum vessel. The white coating on the discs is Gd_2O_3, a strong neutron absorber. w/R corresponds to 12°.

Table 1
Comparison of the time resolution (FWHM) and duty cycle for time-resolved SANS measurements made with the continuous-beam mode (CW) and with TISANE.

The chopper-to-sample distance, L_1 = 15.2 m, sample-to-detector distance, L_2 = 13.5 m, wavelength, λ = 6 Å, and wavelength spread, Δλ/λ = 12 %, are the same for both sample frequencies. C1 and C2 are the rotational frequencies of the two chopper discs. The numbers in bold correspond to the conditions for the TISANE measurements in Fig. 6(*a*).

				TISANE		CW	
N	*M*	C1 (r min^{-1})	C2 (r min^{-1})	δ*t* (μs)	Duty cycle (%)	δ*t* (μs)	Duty cycle (%)
Sample frequency, f_s = 690 Hz							
1	1	3249	3249	**270**	9.9	2462	100
1	2	6499	3249	180	6.6	2462	100
2	3	9748	6499	110	4.0	2462	100
Sample frequency, f_s = 425 Hz							
1	1	2000	2000	440	9.9	2462	100
1	2	4000	2000	290	6.6	2462	100
2	3	6000	4000	**175**	4.0	2462	100

resolution improved, by increasing *N* and *M*, but with a concomitant reduction in the duty cycle.

Table 1 compares the time resolution and relative intensity of time-resolved measurements made both with the continuous-beam mode and with TISANE. For the continuous-beam mode, the time resolution is given by

$$\Delta t(\text{continuous}) = \frac{L_2}{\Delta v_n} = \frac{L_2 m_n \lambda}{h}\frac{\Delta\lambda}{\lambda} = \frac{L_2\lambda}{3.956\ \text{m\AA}\ \text{ms}^{-1}}\frac{\Delta\lambda}{\lambda} \tag{11}$$

where *h* is Planck's constant and m_n is the mass of the neutron. Note that equation (11) is independent of the sample frequency. The TISANE resolution is given by equation (9).

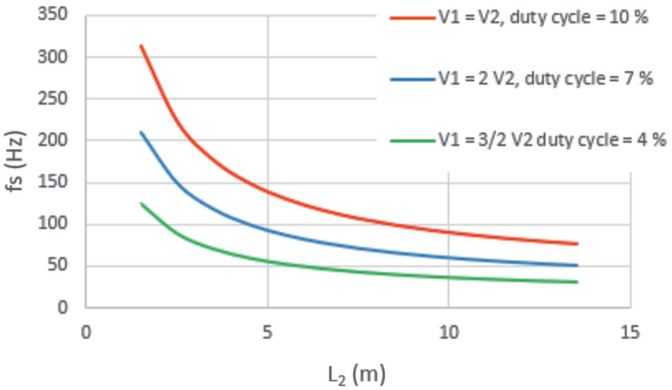

Figure 8
The curves correspond to values L_2, f_s where the time resolution obtainable with continuous-beam time-resolved measurements matches that obtainable with TISANE. For all values of L_2 and f_s above a given curve, the TISANE resolution is better, the more so the farther from the curve. For L_2, f_s values below the curves, *i.e.* at lower frequencies and shorter detector distances (larger *Q* measurements), continuous-mode measurements are preferable, due primarily to their 100% duty cycle. The graph serves as a guide to when the TISANE installation at the NCNR provides an advantage over continuous time-resolved measurements.

Fig. 8 presents another way of comparing the time resolution obtainable with CW and TISANE measurements at NIST. The curves trace the values of detector distance and sample stimulus frequency (L_2, f_s) at which the time resolution of both techniques is the same, for three specific chopper speed ratios, 1/1, 1/2 and 2/3. For L_2, f_s points above each curve, TISANE provides superior time resolution. Fig. 8, therefore, serves as a guide to the trade-offs between the two techniques.

APPENDIX *B*
TISANE electronics

As mentioned in the text, the frequency relationship $f_d = f_s - f_c$, equation (1), must be maintained to high precision over the course of a measurement which might take several hours. A drift in any of these frequencies will result in the mis-encoding of arrival times at the detector and thus broaden and eventually wash out the time dependence of the scattering.

The approach taken at the NCNR to ensure that equation (1) is satisfied has been to continuously monitor the neutron pulse frequency, f_c, and the sample stimulus frequency, f_s, and recalculate f_d as needed to satisfy equation (1). This approach is implemented through a custom piece of electronics, referred to as the DTG.

The chopper control electronics (Lindenau, 2003) output a sharp timing pulse, with frequency f_c, when the openings in the counter-rotating chopper discs coincide at the beam position. These pulses are fed to the DTG, as indicated schematically in Fig. 9, to start a timer. The DTG can also receive narrow pulses, with frequency f_s, marking the start of a sample stimulus cycle. When a sample stimulus pulse is received, the first timer is stopped and its value, Δt_1, corresponding to the time interval between the chopper and sample pulses, is used to compute a second time interval, Δt_2, which is loaded into a count-down timer. The interval $\Delta t_2 = (L_2/L_1)\,\Delta t_1$ to satisfy the TISANE time-focusing conditions depicted in Fig. 10. When

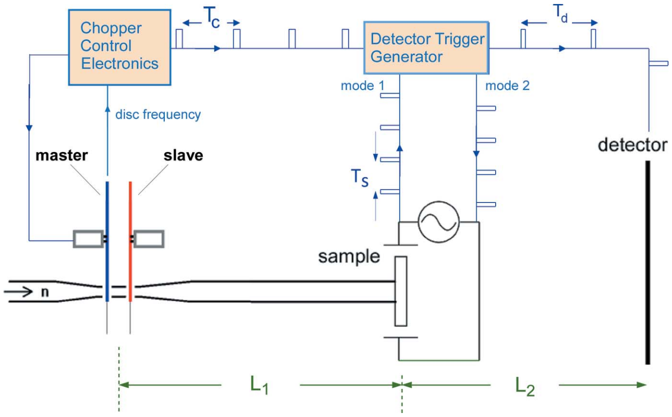

Figure 9
Schematic of the communication scheme between the chopper control electronics, the DTG and the SANS detector. The DTG can either receive pulses from the sample stimulus apparatus (mode 1) or generate pulses to drive the sample stimulus (mode 2). In either mode the DTG sends out pulses to re-zero time stamping of events at the detector.

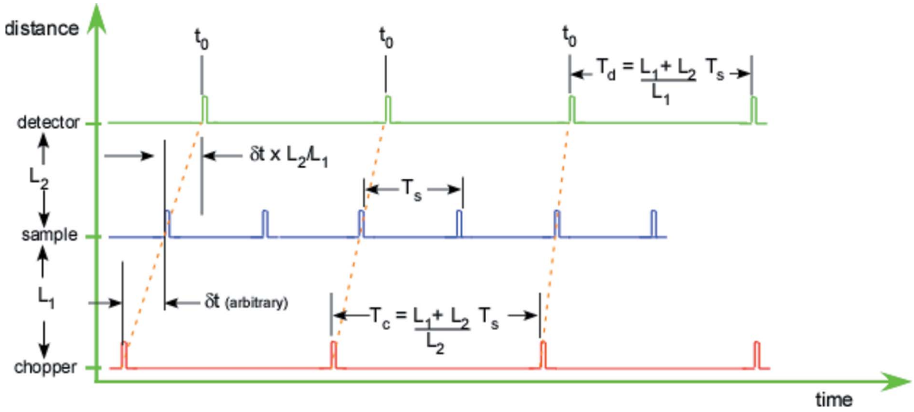

Figure 10
Schematic of the timing relationships between the input (chopper and sample) pulses to the DTG and the output pulses that initiate detector counting cycles. This diagram is drawn for the ratio of $L_2/L_1 = 7/8$. Each t_0 pulse is output based on the most recent pair of chopper and sample pulses. In this way the required TISANE condition, $f_d = f_s - f_c$, is maintained throughout a measurement.

the count-down timer reaches zero, an output pulse (trigger) is sent to the SANS detector to initiate a counting cycle. In this way the detector counting cycle frequency, f_d, is dynamically adjusted to satisfy equation (1) on the basis of the most recent chopper and sample stimulus pulses.

The DTG utilizes a 16-bit MicroChip PIC24FJ64GA002 microcontroller programmed with MicroChip's assembler. This processor was selected for its hardware binary multiplication (16 bits) and its interrupt service calls based on edge of signal at an input. The DTG has front panel switches to select the mode of operation and to input the ratio, L_2/L_1, in 4 byte hexadecimal notation. These are the only inputs required to enable the DTG to send out the detector t_0 pulses at the appropriate time to satisfy the TISANE conditions. The microcontroller has four built-in timers to accomplish its various tasks. The timers have a time step of 0.548 µs per count. The microprocessor's hardware interrupts along with timers are used to measure the T_c and T_s time periods.

A time–distance diagram of the operation of the DTG in mode 1 is shown in Fig. 10.

Acknowledgements

Several insightful technical discussions with J. Barker are acknowledged, as is the assistance of J. Kryzwon with the experiments. We also appreciate the efforts of P. Butler in fostering this collaboration.

Funding information

The following funding is acknowledged: National Science Foundation (award No. DMR-9986442); National Institute of Standards and Technology, NIST Center for Neutron Research; German Research Foundation (DFG, grant No. DI 1788/2-1).

References

Bender, P., Günther, A., Honecker, D., Wiedenmann, A., Disch, S., Tschöpe, A., Michels, A. & Birringer, B. (2015). *Nanoscale*, **7**, 17122–17130.

Glinka, C. J., Barker, J. G., Hammouda, B., Krueger, S., Moyer, J. J. & Orts, W. J. (1998). *J. Appl. Cryst.* **31**, 430–445.

Kipping, D., Gähler, R. & Habicht, K. (2008). *Phys. Lett. A*, **372**, 1541–1546.

Lindenau, B. E. (2003). Central Technology Division (ZAT) of the Forschungszentrum Juelich (FZJ), Project No. FZJ-ZAT-DZ000442-NIST.

Mühlbauer, S., Pfleiderer, C., Böni, P., Forgan, E. M., Brandt, E. H., Wiedenmann, A. & Keiderling, U. (2009). *Physica B*, **404**, 3231–3234.

Perrin, F. (1934). *J. Phys. Radium*, **5**, 497.

Reufer, M., Dietsch, H., Gasser, U., Hirt, A., Menzel, A. & Schurtenberger, P. (2010). *J. Phys. Chem. B*, **114**, 4763–4769.

Tschöpe, A., Birster, K., Trapp, B., Bender, P. & Birringer, R. (2014). *J. Appl. Phys.* **116**, 184305.

Wagner, J., Märkert, C., Fischer, B. & Müller, L. (2013). *Phys. Rev. Lett.* **110**, 048301.

Wiedenmann, A., Keiderling, U., Habicht, K., Russina, M. & Gähler, R. (2006). *Phys. Rev. Lett.* **97**, 057202.

Wright, A. K. & Baxter, J. E. (1976). *Biophys. J.* **16**, 931–938.

Zákutná, D., Falke, Y., Dresen, D., Prévost, S., Bender, P., Honecker, D. & Disch, S. (2019). *Nanoscale*, **11**, 7149–7156.